11-1993

Coherent Versus Incoherent Ladar Detection at 2.09 μm

Jay A. Overbeck
Rose-Hulman Institute of Technology

Martin B. Mark
U.S. Air Force Academy

Scott H. McCraken
U.S. Air Force

Paul F. McManamon
U.S. Air Force

Bradley D. Duncan
University of Dayton, bduncan1@udayton.edu

Coherent versus incoherent ladar detection at 2.09 μm

Jay A. Overbeck,* MEMBER SPIE
University of Dayton
Center for Electro-Optics
300 College Park
Dayton, Ohio 45469

Martin B. Mark
Scott H. McCracken, MEMBER SPIE
Paul F. McManamon
Wright Laboratory
AARI-2, Electro-Optics Sensors Group
Wright Patterson Air Force Base, Ohio 45433

Bradley D. Duncan, MEMBER SPIE
University of Dayton
Center for Electro-Optics
300 College Park
Dayton, Ohio 45469

Abstract. A 2.09-μm ladar system is built to compare coherent to incoherent detection. The 2.09-μm wavelength is of interest because of its high atmospheric transmission and because it is eyesafe. The 2.09-μm system presented is capable of either a coherent or incoherent operational mode, is tunable in a small region around 2.09 μm, and is being used to look at the statistical nature of the ladar return pulses for typical glint and speckle targets. To compare coherent to incoherent detection the probability of detection is investigated as the primary performance criterion of interest. The probability of detection is dependent on both the probability of false alarm and the probability density function, representing the signal current output from the detector. These probability distributions are different for each detection technique and for each type of target. Furthermore, the probability of detection and the probability of false alarm are both functions of the dominating noise source(s) in the system. A description of the theoretical expectations of this system along with the setup of the ladar system and how it is being used to collect data for both coherent and incoherent detection is presented.

Subject terms: acquisition; tracking; pointing; coherent detection; incoherent detection; eye safety; solid state ladar.

Optical Engineering 32(11), 2681–2689 (November 1993).

1 Introduction

Ladar (laser detection and ranging), commonly referred to as "laser radar" or lidar (light detection and ranging), is an extension of conventional radar except that the technique uses optical sources (i.e., lasers) emitting in the near-, mid-, and far-infrared portions of the electromagnetic spectrum, rather than radio wave sources that operate in the microwave portion of the spectrum.[1,2] Ladar wavelengths commonly used today are 10.6 μm (CO_2), 1.06 μm (Nd:YAG) and, recently, 2 μm (Tm, Ho:YAG), where the information in parentheses indicates the appropriate gain medium used for the indicated wavelengths. The 2-μm wavelength is of interest for ladar applications because it is eyesafe, has high atmospheric transmission, and because recent technology has allowed the construction of highly efficient, lightweight, solid state 2-μm ladar systems.

For a system to be considered eyesafe, direct exposure to the transmitted laser beam must not damage the eye under normal conditions. Different parts of the eye are sensitive to different wavelengths of light. For example, the retina is sensitive to visible light (400 to 700 nm) and IR-A (700 to 1400 nm) radiation, whereas, the lens, aqueous humor, and cornea absorb UV (200 to 400 nm), IR-B (1.4 to 3 μm), and IR-C (3 to 1000 μm) wavelengths. At 2.09 μm, the cornea absorbs about 75% of the incident energy, while the remaining 25% is absorbed by the aqueous humor. The primary mechanisms, then, by which the eye may be damaged by 2.09-μm radiation are excess heat generation in the mostly water-based aqueous humor and, more importantly, the formation of corneal cataracts.[3] Limits must therefore be set with regard to exposure duration and intensity so as to minimize eye damaging effects.

The American National Standards Institute (ANSI) has issued standards for maximum permissible exposure (MPE), which is defined as the radiant exposure that individuals may receive without harmful biological effects.[3] For our system (see Fig. 1, which is more fully described later) with a typical output energy of 15 mJ, a pulse duration of 500 ns, and a beam diameter of 5.66 cm at the exit aperture of the telescope,

*Current affiliation: Technology/Scientific Services, Inc., P.O. Box 3065, Overlook Branch, Dayton, Ohio 45431

Paper TPA-18 received April 12, 1993; revised manuscript received June 1, 1993; accepted for publication June 15, 1993.

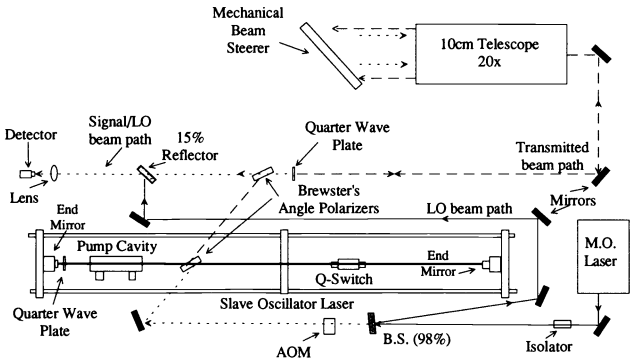

Fig. 1 Experimental setup of the 2.09-μm ladar system.

the radiant exposure an individual would receive by glancing into the exit aperture of the telescope for a single pulse would be 0.6 mJ/cm^2. This is only 4% of the signal pulse MPE of 14.9 mJ/cm^2 for this system, according to ANSI standards.[3] To assess the effects of extended exposure to 2.09-μm radiation, the laser hazard assessment program LHAZ, developed by Armstrong Laboratory according to ANSI standard 136.1-1986, has been used.[4] According to this program, an individual could stare directly into the exit aperture of the telescope of our system (see Fig. 1) for 8.3 h and receive only 68% of the extended MPE of 71.5 J/cm^2. Our 2.09-μm ladar system is thus considered to be eyesafe with respect to the transmitted laser radiation. By contrast, using the same pulse duration, beam diameter, and pulse energy, the single-pulse MPE was calculated[4] for 1.06-μm radiation to be 5 μJ/cm^2. The actual radiant exposure from a single pulse (0.6 mJ/cm^2) would thus be enough to damage the eye at this wavelength. For this reason, a comparable 1.06-μm ladar system would not be considered eyesafe.

The transmitted beams of CO_2 ladars, under the same conditions as considered for the 2.09-μm system, are also eyesafe because the single-pulse MPE is[4] the same as for 2.09 μm. However, even though CO_2 ladars commonly have very high electrical efficiencies (i.e., output optical power versus input electrical power), such systems typically require heavy rf power supplies and detectors cooled with liquid nitrogen. Recent diode technology, however, has allowed a continuously tunable 2.09-μm solid state ladar system to be built. Being solid state in nature, the electrical efficiency of 2-μm ladar systems can approach that of comparable CO_2 systems, yet they are also relatively light weight, and detectors are available that do not require cooling.[5]

A solid state, 2.09-μm ladar system has been assembled to compare the trade-offs between coherent (i.e., heterodyne) detection and incoherent (i.e., direct) detection at 2.09 μm for both glint and speckle targets. The comparison is made based on the probability of detection for each detection scheme because an analysis of this type has not yet been performed for an eyesafe coherent solid state ladar system. This paper describes the experimental arrangement of the ladar system used to compare the detection techniques and the theory used to find the probability of detection. The theoretical analysis begins with a general description of the probability of detection and the probability of false alarm. The discussion then proceeds with a description of the dominant noise sources present in the system and an analysis of the probability of false alarm. Finally, the two detection schemes are compared using the probability of detection for two different types of targets.

2 Experimental Ladar System

The ladar system being used for this work is shown in Fig. 1. This system includes a solid state, continuous wave, 2-μm laser, which is referred to as the master oscillator (MO). The MO signal passes through an optical isolator to isolate the laser from back reflections off of optics further along the beam path. The signal is then split using a 98% beamsplitter. The majority of the MO signal is used as the local oscillator (LO) signal when the system is used in a coherent detection mode. The remaining portion of the beam is frequency shifted 27.1 MHz by an acousto-optic modulator (AOM) and the first diffracted order from the AOM is injected into the transmitter laser [also called the slave oscillator (SO)] to establish injection seeding.

The SO is a flash-lamp-pumped, *Q*-switched laser that uses a chromium (Cr), thulium (Tm), holmium (Ho):YAG crystal as its gain medium. The output coupling of this laser is controlled with the combination of a quarter-wave plate, seen between the end mirror and the pump cavity, and a thin-film Brewster's angle polarizer, seen to the right of the pump cavity. The light traveling to the left in the cavity is horizontally polarized when it strikes the quarter-wave plate. The quarter-wave plate converts the incident linearly polarized light into elliptically polarized light. The elliptically polarized light, on striking the end mirror, reverses its direction of rotation. The light once again passes through the quarter-wave plate and the elliptically polarized light becomes linearly polarized, but it is no longer purely horizontally polarized, now having a small vertically polarized component. The magnitude of the vertically polarized component is dependent on the rotational position of the quarter-wave plate. The vertically polarized light is then reflected out of the cavity by the Brewster's angle polarizer, while the right-hand side of this polarizer is used to inject the frequency-shifted MO signal into the SO cavity for injection seeding. The pulsed SO laser has a repetition rate of 2.7 Hz. The *Q*-switched, injection seeded output of the SO can be monitored using a joulemeter and a typical output energy is 15 mJ. Because of injection seeding, the output is frequency shifted by 27.1 MHz from the LO, allowing for heterodyne detection when desired.

The vertically polarized transmitted output is then reflected off a Brewster's angle polarizer and passes through a quarter-wave plate. The combination of the Brewster's angle polarizer and the quarter-wave plate will be referred to as the transmit-receive switch. The light once transmitted through the quarter-wave plate is left-circularly polarized. This circularly polarized light is reflected into the telescope, where it is expanded into an 8-cm beam and then transmitted to the target using a mechanical beam steerer. Ideally, the transmitted left-circularly polarized light will reverse its direction of rotation on reflection from a target, producing right-circularly polarized light. The depolarization effects of the target vary depending on the type of target, but the overall effect of the depolarization of the return signal is a decrease in the received SNR. Based on tabulated results from 10.6-μm data, we expect to receive 80% of the light in the right-

circularly polarized state, which corresponds[1] to a loss of only 0.7 dB. Because there is a lack of data for depolarization at 2 μm, the effects are ignored for this analysis.

The return scatter is collected by the same telescope, transmitted through the transmit-receive switch, and then through a 15% beamsplitter after which it is focused onto a photodetector. When coherent detection is desired, the LO is mixed with the return signal at the 15% beamsplitter, whereas for incoherent detection, the LO is simply blocked.

To effectively compare the two detection techniques, the focal length of the lens used to focus the return signal onto the detector needs to reach the optimum level for each detection scheme. Because optimum detection does not occur with the same collection optics, two different lenses are needed, one for each detection technique. For incoherent detection, optimum detection occurs when all of the collected light impinges on the detector, where, in the detector plane, the received light is transformed by lens diffraction into an Airy disk pattern. For this work, considering the optics on hand and the beam diameter, a lens was chosen that focused the central lobe and the first ring of the Airy disk pattern onto the detector[6] ($f=50$ mm).

For coherent detection, the optimum detection occurs with a high heterodyne efficiency. The heterodyne efficiency is a ratio that expresses how efficiently the return signal and the LO mix spatially. When the return signal and the LO are matched Airy functions at the plane of the detector, the heterodyne efficiency γ is given by[6,7]

$$\gamma = 1 - J_0^2(x) - J_1^2(x) \ , \tag{1}$$

where $x = \pi rD/f\lambda$, f is the focal length of the lens, D is the diameter of the laser beam, λ is the wavelength, r is the radius of the detector, and J_0 and J_1 are Bessel functions of the first kind. Equation (1) is plotted in Fig. 2. For our system, the radius of the detector r is 50 μm, λ is 2.09 μm, and the diameter of the laser beam D is 4 mm. Note that the smaller the focal length lens chosen, the better the heterodyne efficiency. For our work, a reasonable focal length lens of 80 mm was chosen, giving an x of 3.75 and a theoretical heterodyne efficiency of 0.84 (see Fig. 2).

A schematic of the detection packages provided by Coherent Technologies, Inc. (CTI) of Boulder, Colorado, is shown in Fig. 3. The photodetector is reversed biased V_R by a 3-V battery and is in series with a 1-kΩ resistor. The photodetector used is a *p-i-n* InGaAs photodiode, which has a measured dark current of 135 nA and responsivity of 1.1 A/W at 2.09 μm. Because for coherent detection the detected signal will be at high frequencies, 27.1 MHz, and for direct detection the detected signal will be at low frequencies, 2.7 Hz, the postdetection electronics are different for each detection scheme. For incoherent detection, the amplifier was purchased from Analog Modules and it has[8] a bandwidth of 35 MHz and a midband gain of 60 dB. There are no filters used for the incoherent detection scheme so the bandwidth is limited by the amplifier. The optimum load resistance R_L found[9] by CTI for incoherent detection is 16 MΩ.

For the heterodyne detection case, the same reverse bias voltage, series resistance, and photodiode are used (see Fig. 3). The amplifier, provided by Miteq, has a bandwidth of 100 MHz and a midband gain of 47 dB (Ref. 10). To limit the bandwidth of the detection package and to isolate the return signal, a 41-MHz bandpass filter centered at the intermediate frequency, 27.1 MHz, was used.[9] The load resistance R_L found by CTI for optimized heterodyne detection for this system at 27.1 MHz is 450 Ω (Ref. 9).

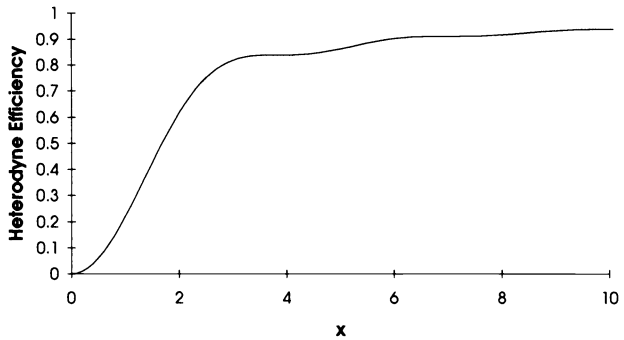

Fig. 2 Heterodyne efficiency for matched signal and LO Airy functions incident on the detector. The expression for the heterodyne efficiency used to plot this curve is $\gamma = 1 - J_0^2(x) - J_1^2(x)$.

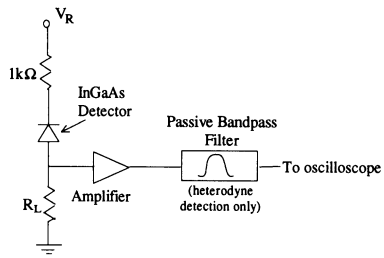

Fig. 3 Detection scheme used with the 2.09-μm ladar system. When this detection package is used for incoherent detection the amplifier is a 60-dB amplifier, R_L is 16 MΩ, and there is no bandpass filter. When used for coherent detection the amplifier is a 47-dB amplifier, R_L is 450 Ω, and the bandpass filter is 41 MHz.

3 Theory

Coherent to incoherent detection is compared assuming both a speckle and a glint target. The basis for this comparison is the probability of detection. To understand the probability of detection, the role of the statistical nature of the noise and the return signal plus noise must first be understood. The noise distribution shown [11] in Fig. 4 is the probability density function (PDF), which represents, generally, the fluctuation of the postdetection noise current in a radar system when there is no target present. The shape and the position of this probability distribution is dependent on the detection technique used and on the average value of the noise current I_{noise}. When a signal is present, the average value of the signal current I_{signal} is generally greater than the average value of the noise current, so that the PDF representing the fluctuation in the combined return signal current, plus noise current, is centered about an average value of $I_{\text{signal}} + I_{\text{noise}}$. The second distribution shown in Fig. 4 represents, generally, the sum of the signal and noise current.

To decide whether a value measured by the detector is from an actual target or whether it is noise, a threshold current $I_{\text{threshold}}$ is set, as shown in Fig. 4. Whenever a current produced by the detector is larger than the threshold current, a

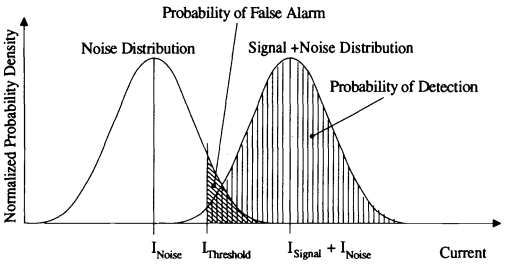

Fig. 4 Probability of false alarm and the probability of detection for a given threshold current level. The noise distribution is centered at the average noise current and the signal plus noise distribution is centered at the average signal plus noise current.

target is said to have been detected. Whether or not a real target exists has yet to be determined. The probability that a target has been detected is called the probability of detection, which is, mathematically, the area under the PDF for the signal and noise greater than the set threshold. There is also the probability that the current produced by the detector exceeds the threshold caused by noise effects only. The probability of this occurring is called the probability of false alarm and is, mathematically, the area under the noise current distribution greater than the set threshold current.

To find the probability of detection for the 2.09-μm ladar system the average value of the dominating noise source(s) needs to be determined, as is discussed in the following section. The PDF that the dominating noise source(s) exhibits is then discussed for both coherent and incoherent detection. The probability distributions of the noise are then used in conjunction with desired probabilities of false alarm to find the needed threshold for that false alarm rate. These threshold values are then used with the PDFs representing the detector output current to calculate the probability of detection. The distributions representing the fluctuation in the detector output current are different for each type of target and for each detection scheme. The results of the probability of detection for each of the targets and for each detection technique are then compared.

3.1 *Average Noise*

The noise sources of concern for the 2.09-μm ladar system are essentially the same for either incoherent or coherent detection. These noise sources are dark current noise, Johnson or thermal noise, background noise, and shot noise, where equations for the mean-squared values of these noise sources are shown[12,13] in Table 1. Because the detection package is optimized differently for coherent detection than for incoherent detection, the values for the variables used in the noise expressions are different for each detection technique. The values for the majority of these variables were found in data sheets provided by the manufacturers[8,9,13] and are listed in Table 2. In the case of background noise, the value for the solar backscatter P_{SB} was calculated assuming the worst-case scenario, which is a ladar looking at a sun-illuminated cloud.[1,13] The parameters used to calculate the solar backscattered power are tabulated values listed in Ref. 13. As for shot noise, the value of the average detector current is different for the coherent detection and incoherent detection cases. When using incoherent detection, the shot noise is produced only by the return power from the target incident

Table 1 Dominating noise sources in a 2.09-μm ladar system.

Noise Source	Expression	Variables
Dark current	$\langle i_{Dk}^2 \rangle = 2qI_{Dk}B$	q= charge on an electron = 1.602×10^{-19} C I_{Dk} = average dark current of detector B= bandwidth of detection electronics [8,9] k= Boltzman's constant = 1.38×10^{-23} J/K T= temperature = 293 K R_L = load resistor [9] P_{SB} = amount of solar backscatter (measured in Watts) seen by detector [13] R_{Det} = responsivity of detector I_D = average detector current $=R_{Det}P_0$, where P_0 is the power incident on the detector
Thermal	$\langle i_J^2 \rangle = \frac{4kTB}{R_L}$	
Background	$\langle i_{Bk}^2 \rangle = 2qBP_{SB}R_{Det}$	
Shot	$\langle i_{SN}^2 \rangle = 2qI_DB$	

Table 2 Numerical values for the variables listed and defined in Table 1.

Variable	Detection Scheme	
	Coherent	Incoherent
B	41 MHz	35 MHz
I_{Dk}	135 nA	135 nA
T	293 K	293 K
R_L	450 Ω	16 MΩ
P_{SB}	1.58×10^{-10} W	1.58×10^{-10} W
R_{Det}	1.1 A/W	1.1 A/W
P_O	1.0 mW	250 nW
I_D	1.38 mA	275 nA

on the detector. Using the radar range equation,[1] the return power for a diffuse target for this system is of the order of 250 nW. For coherent detection, 1.0 mW of local oscillator power is used to produce a shot noise current that is 10 dB above the dominating noise current, which ensures LO shot-noise-limited detection. These values of incident power on the detector and the currents produced by the detector are also listed in Table 2.

The amplifiers also contribute noise to the measured signal. The amount of noise produced by the respective amplifiers was measured for both coherent and incoherent detection schemes by attaching the effective input impedance seen by the amplifier to the input of the amplifier. The output of the amplifier was then monitored using a spectrum analyzer. The average noise level seen on the spectrum analyzer was measured. Taking into account the bandwidth of each of the respective detection circuits and the input impedance of the spectrum analyzer, the mean-squared noise current was found. The measured amplifier noise current levels are given in Table 3 along with the calculated values of the other noise current terms.

From Table 3, the dominating noise source for incoherent detection is seen to be the amplifier noise (7.0×10^{-15} A^2). This is used as the mean-squared noise current, $\langle i_{NI}^2 \rangle$, for incoherent detection throughout the rest of this paper. For coherent detection the dominating mean-squared noise $\langle i_{NC}^2 \rangle$ is the local oscillator shot noise (1.5×10^{-14} A^2). Likewise, this value is used throughout the rest of the paper as the mean-squared noise current when referring to coherent detection.

3.2 *Probability Density Functions of Dominating Noise Terms*

The fluctuations of current in the detection circuit are caused by the detection process and other noise sources as described

Table 3. Evaluation of the noise sources in the ladar system. These values were calculated using the equations in Table 1 for the specific characteristics of the 2.09-μm ladar system.

Noise Source	Detection Scheme	
	Coherent	Incoherent
Dark current	1.77×10^{-18} A^2	1.51×10^{-18} A^2
Thermal	1.47×10^{-15} A^2	3.54×10^{-20} A^2
Background	2.28×10^{-21} A^2	1.95×10^{-21} A^2
Shot	1.50×10^{-14} A^2	3.08×10^{-18}A^2
Amplifier	7.04×10^{-20} A^2	7.00×10^{-15} A^2

earlier. These fluctuations, being random, can be expressed using probability density functions (PDFs). Each of the detection techniques has a PDF representing the probability distribution of the primary noise source. Using these distributions, equations for the probability of false alarm can be found.

For incoherent or direct detection, the dominating noise term was found to be thermal noise produced by the amplifier. The thermal noise current fluctuation is easily modeled as a Gaussian distribution.[12,14] The incoherent Gaussian noise current distribution $P_{\text{in}}(i)$ can be expressed as

$$P_{\text{in}}(i)=\frac{1}{(2\pi\langle i_{\text{NI}}^2\rangle)^{1/2}}\exp\left(-\frac{i^2}{2\langle i_{\text{NI}}^2\rangle}\right), \tag{2}$$

where i is the instantaneous detector output current and $\langle i_{\text{NI}}^2\rangle$ is the mean-squared noise current for incoherent detection.

For the heterodyne or coherent detection case, the received signal will be at an intermediate frequency. The best process by which to detect this signal is envelope detection. The dominant noise in this case is local oscillator shot noise and the fluctuations in the envelope-detected noise current can be described by a Rayleigh PDF, $P_{\text{CO}}(i)$, given by[14]

$$P_{\text{co}}(i)=\frac{i}{\langle i_{\text{NC}}^2\rangle}\exp\left(-\frac{i^2}{2\langle i_{\text{NC}}^2\rangle}\right), \tag{3}$$

where $\langle i_{\text{NC}}^2\rangle$ is the mean-squared noise current for coherent detection.

3.3 *Probability of False Alarm*

A false alarm occurs when the return signal exceeds the threshold when there is no target present. For a given threshold level, the probability of false alarm is the probability that the noise level will exceed that threshold level. Mathematically it is defined as the area under the noise PDF that exceeds the set threshold level i_T. To find the probability of false alarm, the area under the noise probability density curve is calculated from the threshold level to infinity (see Fig. 4). The probability of false alarm for incoherent detection $P_{\text{in}_{\text{FA}}}$ is

$$P_{\text{in}_{\text{FA}}}=\int_{i_T}^{\infty}p(i)\,\mathrm{d}i=\frac{1}{(2\pi\langle i_{\text{NI}}^2\rangle)^{1/2}}\int_{i_T}^{\infty}\exp\left(\frac{-i^2}{2\langle i_{\text{NI}}^2\rangle}\right)\mathrm{d}i$$

$$=0.5\ \text{ERFC}\left[\frac{i_T}{(2\langle i_{\text{NI}}^2\rangle)^{1/2}}\right], \tag{4}$$

where the complementary error function ERFC(x), is defined as

$$\text{ERFC}(x)=\frac{2}{\sqrt{\pi}}\int_x^{\infty}e^{-t^2}\,\mathrm{d}t\ .$$

The probability of false alarm for the coherent case P_{coFA} is then

$$P_{\text{coFA}}=\int_{i_T}^{\infty}p(i)\,\mathrm{d}i=\exp\left(\frac{-i_T^2}{2\langle i_{\text{NC}}^2\rangle}\right). \tag{5}$$

Now that the equations for the probability of false alarm have been found, they can be manipulated using the threshold current variable i_T to obtain desired probabilities of false alarm. The value of the threshold current used to determine the desired probability of false alarm can then be used to find the probability of detection, as shown in the following.

3.4 *Probability of Detection*

The probability of detection is the probability that the signal exceeds a set threshold when a target is present. Mathematically speaking, the probability of detection is the area under the probability density function representing the signal and noise greater than the decision threshold (see Fig. 4). The probability density functions are different for each detection scheme and for each type of target. The types of targets of interest are a speckle, or diffuse target, and a glint target, which produces a specular reflection off the target. Because there are two detection techniques of interest and two targets of interest, the following discussion is divided into four sections. Each section presents the probability distribution for a specific detection scheme for an individual type of target.

3.4.1 *Coherent detection with a diffuse/speckle target*

A diffuse target is by definition optically rough and scatters incident light randomly. When viewed, the scattered light from a diffuse target resembles random light and dark patches. The current produced by the detector viewing this random pattern will have a Gaussian distribution.[2] Because both the signal and the noise currents are represented by Gaussian PDFs, their combination can be represented by a Gaussian PDF, where the variance is equal to the sum of the signal and noise current variances. With coherent detection, the envelope-detected Gaussian-distributed signal will have[15] a Rayleigh PDF. Therefore, the PDF for coherent detection with a speckle target p_{CS} is given as

$$p_{\text{CS}}(i)=\frac{i}{\langle i_{\text{NC}}^2\rangle+\langle i_{\text{diffuse}}^2\rangle}\exp\left[\frac{-i^2}{2(\langle i_{\text{NC}}^2\rangle+\langle i_{\text{diffuse}}^2\rangle)}\right], \tag{6}$$

where i represents the instantaneous peak envelope detected signal and $\langle i_{\text{diffuse}}^2\rangle$ represents the as yet unspecified mean-squared signal current from a diffuse target.

The probability of detection for this case, Pd_{CS}, is then

$$Pd_{\text{CS}}=\int_{i_T}^{\infty}p_{\text{CS}}(i)\,\mathrm{d}i=\int_{i_T}^{\infty}\frac{i}{\langle i_{\text{NC}}^2\rangle+\langle i_{\text{diffuse}}^2\rangle}$$

$$\times \exp\left[-\frac{i^2}{2(\langle i_{NC}^2\rangle + \langle i_{diffuse}^2\rangle)} \right] di$$

$$= \exp\left[-\frac{i_T^2}{2(\langle i_{NC}^2\rangle + i_{diffuse}^2\rangle)} \right] . \quad (7)$$

Equation (7) is then rewritten to make explicit SNR $= \langle i_{diffuse}^2\rangle / \langle i_{NC}^2\rangle$. That is,

$$Pd_{CS} = \exp\left[-\frac{i_T^2/\langle i_{NC}^2\rangle}{2(1+\langle i_{diffuse}^2\rangle/\langle i_{NC}^2\rangle)} \right] . \quad (8)$$

To calculate the probability of detection, one first has to choose a desired probability of false alarm. Probability of false alarms were arbitrarily chosen in the range from 1×10^{-2} to 1×10^{-10} to give a general idea of the changes that occur in the shape of the curves representing the probability of detection with different probabilities of false alarm. Using these given values for the probabilities of false alarm, a threshold value can be backed out using the equation for the probability of false alarm for coherent detection, which is given in Eq. (5). Using Eq. (5), a probability of false alarm of 1×10^{-2} and 1.5×10^{-14} A^2 as the mean-squared noise current (see Table 3), a threshold of 371.7 nA was found. This threshold was then used in Eq. (8) to find the probability of detection for coherent detection with a speckle target for a range of SNRs. Figure 5 shows Pd_{CS} for different probabilities of false alarm for a range of SNR in decibels.

3.4.2 *Coherent detection with a glint target*

A glint or specular target produces a deterministic nonstatistically varying return.[2] The combination of this return signal and the Gaussian noise gives a complex Gaussian distribution for the overall detected current. The return is complex because there are both in-phase and out-of-phase components because of differences in range to the target. The PDF representing the envelope of the current fluctuations (signal and noise) at the output of the bandpass filter (see Fig. 3) for coherent detection with a glint target, p_{CG}, is given by[2,11,14,15]

$$p_{CG}(i) = \frac{2i}{\langle i_{NC}^2\rangle} \exp\left(-\frac{i_{glint}^2 + i^2}{\langle i_{NC}^2\rangle} \right) I_0\left(\frac{2i_{glint} i}{\langle i_{NC}^2\rangle} \right) . \quad (9)$$

This is known as the Rician probability density function where I_0 is the zeroth-order modified Bessel function of the first kind, i_{glint} is the amplitude of the signal from a glint target, and $\langle i_{NC}^2\rangle$ is the mean-squared noise current for coherent detection. The probability of detection Pd_{CG} is then given by

$$Pd_{CG} = \int_{i_T}^{\infty} \frac{2i}{\langle i_{NC}^2\rangle} \exp\left(-\frac{i_{glint}^2 + i^2}{\langle i_{NC}^2\rangle} \right) I_0\left(\frac{2i_{glint} i}{\langle i_{NC}^2\rangle} \right) di . \quad (10)$$

Equation (10) can be rearranged so it is a function of the SNR, $i_{glint}^2/\langle i_{NC}^2\rangle$, which is

$$Pd_{CG} = \int_{i_T}^{\infty} \frac{2i}{\langle i_{NC}^2\rangle} \exp\left[-\left(\frac{i_{glint}^2}{\langle i_{NC}^2\rangle} + \frac{i^2}{\langle i_{NC}^2\rangle} \right) \right] I_0\left(\frac{2i_{glint} i}{\langle i_{NC}^2\rangle} \right) di . \quad (11)$$

Using the same threshold currents calculated from Eq. (5), which was done for the coherent detection speckle target case, the integral in Eq. (11) for the probability of detection can be numerically integrated. Figure 6 shows the probability of detection versus SNR for the glint target.

3.4.3 *Incoherent detection with a glint target*

For incoherent detection, both the return signal and the noise (amplifier noise limited for us), at the output of the detector, for a large photoelectron count rate, have[14] independent Gaussian PDFs. Therefore, the PDF representing the combination of the return signal and noise for this case is a Gaussian where the mean is equal to the amplitude of the current produced by the glint return and the variance is the sum of the independent signal and noise current variances. The PDF representing the fluctuation in the current for incoherent detection with a glint target p_{IG} is[14]

$$p_{IG} = \frac{1}{[2\pi(\langle i_{NI}^2\rangle + \langle i_{glint}\rangle)]^{1/2}} \exp\left[-\frac{(i-\langle i_{glint}\rangle)^2}{2(\langle i_{NI}^2\rangle + \langle i_{glint}\rangle)} \right] , \quad (12)$$

where $\langle i_{glint}\rangle$ is the average return signal from a glint target and, because the statistics of the return signal are generally Poisson, the variance is equal to the mean.

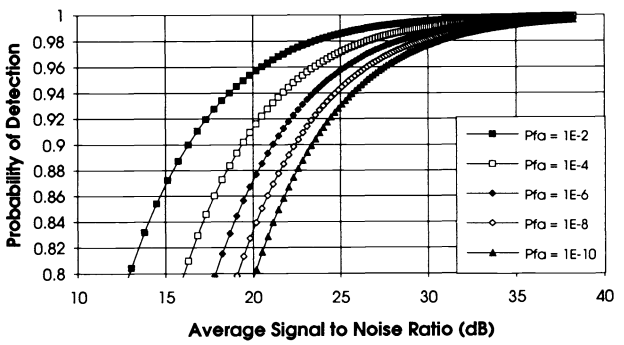

Fig. 5 Probability of detection plotted against SNR for a speckle target using coherent detection. These curves were calculated using threshold currents for decreasing probability of false alarm of 371.7, 525.7, 643.9, 743.5, and 831.3 nA.

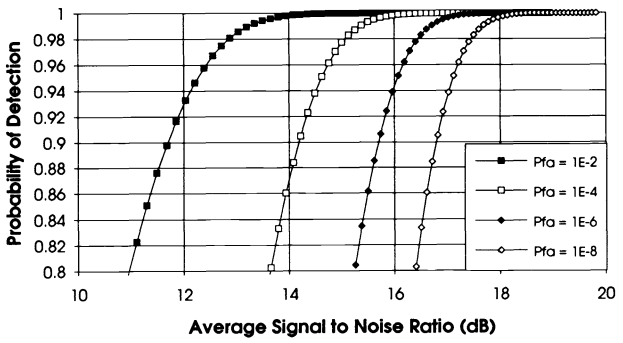

Fig. 6 Probability of detection plotted against SNR for a glint target using coherent detection. The threshold currents used for each curve for decreasing probability of false alarm are 371.7, 525.7, 643.9, 743.5, and 831.3 nA.

The probability of detection Pd_{IG} is then calculated as

$$Pd_{IG}=\frac{1}{[2\pi(\langle i_{NI}^2\rangle+\langle i_{glint}\rangle)]^{1/2}}\int_{i_T}^{\infty}\exp\left[-\frac{(i-\langle i_{glint}\rangle)^2}{2(\langle i_{NI}^2\rangle+\langle i_{glint}\rangle)}\right]di\,. \tag{13}$$

This can be expressed in terms of the error function (ERF) and the complementary error function (ERFC) as

$$Pd_{IG}=0.5\text{ERFC}\left\{\frac{(i_T-\langle i_{glint}\rangle)^2}{[2(\langle i_{NI}^2\rangle+\langle i_{glint}\rangle)]^{1/2}}\right\} \tag{14a}$$

when $i_T-\langle i_{glint}\rangle\geq 0$, and

$$Pd_{IG}=0.5\left(1+\text{ERF}\left\{\frac{(\langle i_{glint}\rangle-i_T)^2}{[2(\langle i_{NI}^2\rangle+\langle i_{glint}\rangle)]^{1/2}}\right\}\right) \tag{14b}$$

when $i_T-\langle i_{glint}\rangle<0$, where ERF($z$) is given as

$$\text{ERF}\ (z)=\frac{2}{\sqrt{\pi}}\int_0^z e^{-t^2}\,dt\,.$$

The probability of detection is calculated similarly to the method used for coherent detection, except the equation for the probability of false alarm is Eq. (4) and the mean-squared noise current $\langle i_{NI}^2\rangle$ is 7.00×10^{-15} A^2 (see Table 3). Figure 7 shows the probability of detection for incoherent detection with a glint target.

3.4.4 *Incoherent detection with a speckle target*

The PDF is a negative binomial distribution for incoherent detection with a speckle target when the return energy from the target is known exactly or it can be calculated exactly.[16] In our case, the return energy on the detector cannot be predicted because of the randomness caused by the surface irregularities in the target. Because the return energy is random, the probability that k signal photoelectrons are produced is given by Goodman[16] as

$$p_{IS}(k)=\int_0^{\infty}P_s(k|W)p(W)\,dW\,, \tag{15}$$

where $p(W)$ is the PDF representing the return energy W from a target incident on the receiver aperture during a pulse; $p(W)$ is given as[16]

$$p(W)=\begin{cases}\dfrac{a^M W^{M-1}\exp(-aW)}{\Gamma(M)} & W\geq 0\\ 0 & \text{otherwise}\,,\end{cases}$$

where M is the number of correlation cells received, a is $M/\langle W\rangle$, $\langle W\rangle$ is the average return energy, and Γ is the gamma function.

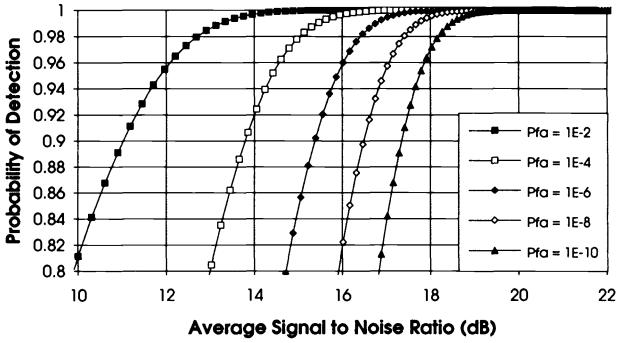

Fig. 7 Probability of detection plotted against SNR for a glint target using incoherent detection. These curves were calculated using threshold currents of 194.7, 311.2, 397.8, 469.7, and 532.4 nA.

The probability $P_S(k|W)$ that k photoelectrons are produced for a given incident energy W is a Poisson distribution given as

$$P_S(k|W)=\frac{(\eta W/h\nu)}{k!}\exp\left(-\frac{\eta W}{h\nu}\right)\,,$$

where $\eta W/h\nu$ is the mean, η is the quantum efficiency of the detector, h is Plank's constant, and ν is the optical frequency. Fortunately, in the presence of a large photoelectron count rate, a Poisson distribution can be approximated as a Gaussian distribution. This Gaussian distribution has the form

$$P_s(k|W)=\frac{1}{[2\pi(\langle n\rangle+bW)]^{1/2}}\exp\left\{-\frac{[k-(\langle n\rangle+bW)]^2}{2(\langle n\rangle+bW)}\right\}\,, \tag{16}$$

where $\langle n\rangle$ is the mean number of noise photons, b is $\eta/h\nu$, and bW represents the number of signal photons. The probability of detection is then

$$Pd_{IS}=\int_{x_T}^{\infty}\int_0^{\infty}P_s(k|W)p(W)\,dW\,dk\,, \tag{17}$$

where x_T is the threshold current in terms of photoelectrons. Figure 8 shows the probability of detection for the incoherent case with a speckle target [Eq. (17)] plotted against SNR for different probabilities of false alarm. The threshold currents used in this case are the same as those found for the incoherent detection glint target case.

4 Analysis of Results

To compare the detection techniques for the different targets, the coherent and incoherent probability of detection curves for the glint target were plotted on the same graph and the same was done for the speckle target. Figure 9 shows the combination of the coherent and incoherent detection curves for a glint target. For probabilities of detection less than 0.96, incoherent detection performs with a lower SNR for a given probability of detection than coherent detection. For high probabilities of detection (>0.96) the curves are basically the same.

Figure 10 shows the comparison between coherent and incoherent detection with a speckle target. As can be seen in

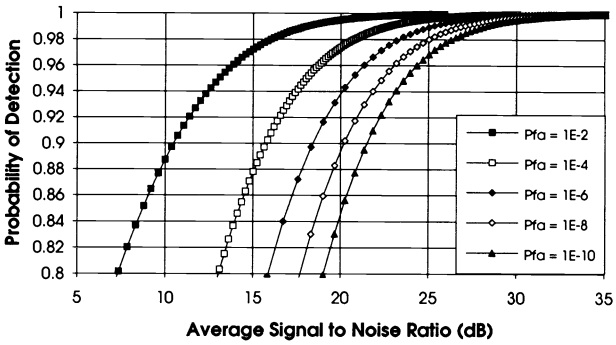

Fig. 8 Probability of detection plotted against SNR for a speckle target using incoherent detection. These curves were calculated using threshold currents of 194.7, 311.2, 397.8, 469.7, and 532.4 nA.

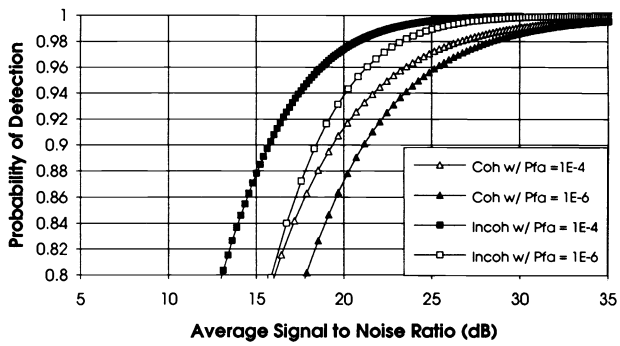

Fig. 10 Comparison of probability of detection for coherent versus incoherent detection with a speckle target. This plot is a combination of Figs. 5 and 8.

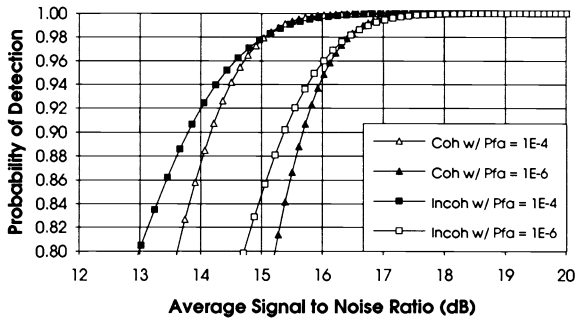

Fig. 9 Comparison of probability of detection for coherent versus incoherent detection with a glint target. This plot is a combination of Figs. 6 and 7.

the figure, the incoherent detection scheme can detect a target with a lower SNR for a given probability of detection than the coherent detection scheme can. This was somewhat unexpected. A possible reason for incoherent detection with a speckle target performing better than coherent detection is that only part of the return power that mixes with the LO is that which is in phase with the LO, whereas all of the return power in the incoherent case is used.

5 Summary

An eyesafe, solid state, 2-μm ladar has been built to perform a comparison between coherent and incoherent detection. The system is presently being used to verify the statistical nature of the laser radar return pulses from a glint and a speckle target. This statistical data will be used to compare the detection schemes using the probability of detection and will be compared to the theoretical predictions presented in this paper in a forthcoming paper. The theoretical results show that for a glint target there is essentially no difference in the detection techniques for high probabilities of detection. Although, for a speckle target, incoherent detection shows a better probability of detection for a given SNR than coherent detection does.

Acknowledgments

Helpful discussions with Richard Richmond of the Wright Laboratory Electro-Optic Sensors Group are gratefully acknowledged. Special thanks also to Mohammad A. Karim and the University of Dayton Research Council for their continuing support of the authors research and scholarly activities. This work has been sponsored by the Wright Laboratory Avionics Directorate and Technology/Scientific Services, Inc., of Dayton, Ohio.

References

1. A. V. Jelalian, *Laser Radar Systems,* Artech House, Norwood, Mass. (1992).
2. C. G. Bachman, *Laser Radar Systems and Techniques,* Artech House, Norwood, Mass. (1979).
3. D. Sliney and M. Wolbarsht, *Safety with Lasers and Other Optical Sources,* Plenum Press, New York (1980).
4. D. P. Beneditz, R. L. Lindsey, and J. A. Labo, "Integrated laser hazard assessment program (LHAZ)," Ver. 2.0, Brooks Air Force Base, Tx. (1992).
5. M. J. Kavaya, A. W. Henderson, E. Russell, R. M. Huffaker, and R. G. Frehlich. "Monte Carlo computer simulations of ground-based and space-based coherent DIAL water vapor profiling," *Appl. Opt.* **28**(5), 840–851 (1989).
6. M. Born and E. Wolf, *Principles of Optics,* p. 398, Pergamon Press, New York (1980).
7. D. Fink, "Coherent detection signal-to-noise," *Appl. Opt.* **14**(3), 689–690 (1975).
8. "Amplifier specifications," Analog Modules, Inc., Longwood, Fla. (1992).
9. "Detection circuits for coherent laser radar," CTI, Boulder, Colo. (1992).
10. "Amplifiers to 2 GHz," Miteq, Hauppauge, N.Y. (1991).
11. M. I. Skolnik, *Introduction to Radar Systems,* McGraw-Hill, New York (1962).
12. A. Yariv, *Optical Electronics,* 3rd ed., Holt, Rinehart and Winston, Inc., New York (1985).
13. RCA, *Electro-Optics Handbook,* Commercial Engineering, Harrison, N.J. (1974).
14. R. H. Kingston, *Detection of Optical and Infrared Radiation,* Springer-Verlag, New York (1978).
15. S. O. Rice, "Mathematical analysis of random noise," *Bell Syst. Tech. J.* **23,** 282–332 (1944); *Bell Syst. Tech. J.* **24,** 46–156 (1945).
16. J. W. Goodman, "Some effects of target-induced scintillation on optical radar performance," *Proc. IEEE* **53**(11), 1688–1700 (1965).

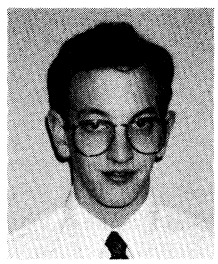

Jay A. Overbeck received his BS degree in applied optics at Rose-Hulman Institute of Technology, Terre Haute, Indiana, in 1991. He is working toward an MS in electro-optics at the University of Dayton, Ohio. Currently, he is doing research with solid state laser radar systems at Wright Laboratory, Wright-Patterson Air Force Base, on contract with Technology/Scientific Services, Inc.

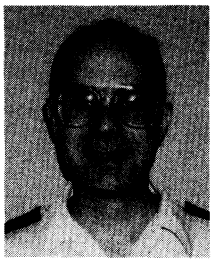

Martin B. Mark received his BS in electrical engineering from Purdue University in 1979, his MSEE from the Air Force Institute of Technology in 1980, and his PhD from the Massachusetts Institute of Technology in 1986. He has been an officer in the U.S. Air Force since graduating from Purdue in 1979. In the Air Force, he has worked on the development of space-based optical communication systems, performed research involving numerous laser radar systems, and taught electrical engineering at the U.S. Air Force Academy. He is currently performing laser radar research at the Air Force Wright Laboratory at Wright-Patterson Air Force Base, Ohio.

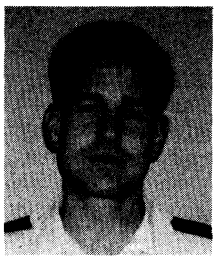

Scott H. McCracken graduated from Rochester Institute of Technology, New York, with a BS in microelectronic engineering. While earning his degree he worked as a co-op student for Hughes Aircraft Co. in Carlsbad, Calif., and IBM in East Fishkill, N.Y., and Manasas, Va. After receiving his commission in the Air Force he went to work in the Avionics Directorate of Wright Laboratory at Wright-Patterson Air Force Base, Ohio. His current work includes solid state laser radar for Air Force applications.

Paul F. McManamon: Biography and photograph of author appear with the paper "Sensitivity improvement of 1-μm ladar system incorporating an optical fiber preamplifier" in this issue.

Bradley D. Duncan: Biography and photograph of author appear with the paper "Sensitivity improvement of a 1-μm ladar system incorporating an optical fiber preamplifier" in this issue.